

Tunable skyrmion crystals and topological quantum oscillations in magnetic metals

Sopheak Sorn,¹ Stefan Divic,¹ and Arun Paramakanti^{1,*}

¹*Department of Physics, University of Toronto, Toronto, Ontario, Canada M5S 1A7.*

(Dated: December 15, 2024)

Skyrmions were first introduced in particle physics as topologically nontrivial field configurations to model nucleons [1]. In a condensed matter setting, skyrmions appear as topological magnetic swirls in quantum Hall systems [2–5], bulk and thin film magnets [6–20], and artificially engineered systems such as magnetic multilayers [21–23] and oxide interfaces [24–26]. Research in this field has led to the discovery of the topological Hall effect in ferromagnetic skyrmion crystals [27, 28] and an ongoing hunt for nanoscale skyrmions in frustrated antiferromagnets [29–33]. In our work, we study the effect of nonlinear mode-mode coupling in skyrmion crystals. For frustrated antiferromagnets, this leads to a theory for short-period Bloch skyrmion crystals in materials like Gd_2PdSi_3 where recent experiments report a giant topological Hall effect [34]. For ferromagnets with Dzyaloshinskii-Moriya interactions, such nonlinearity leads to highly field-tunable Néel skyrmion crystals, realizing a Berry-Hofstadter butterfly and a novel phenomenon we term “topological quantum oscillations”.

In many solid-state materials, such as MnSi , skyrmions occur as crystals — periodic noncoplanar textures from a superposition of multiple spin spirals [9, 10, 12, 17, 27] created by the Dzyaloshinskii-Moriya (DM) exchange interaction which is present in noncentrosymmetric systems. An electron moving in such a spin texture picks up a Berry phase [35–37]. The resulting Berry flux, arising from the scalar spin chirality of the skyrmion crystal, modifies the conventional Hall effect due to an orbital magnetic field and leads to an observed additional “topological Hall effect” contribution [27, 28].

More recently, skyrmion crystals have been discovered in a metallic layered-triangular antiferromagnet Gd_2PdSi_3 [34]. In this systems, the spiral magnetism appears to be favored by frustrated Gd-Gd magnetic exchange couplings on a triangular lattice. In general, such frustrated antiferromagnets can host stronger spin twisting, which may lead to smaller skyrmions and denser information storage. At the same time, they can support a large scalar spin chirality [30, 31, 38] and can even exhibit a quantized topological Hall effect [29–33, 39, 40]. Indeed, recent experiments on Gd_2PdSi_3 , a material where early work had reported a resistivity minimum possibly tied to short-range magnetic correlations [41], have pro-

vided evidence for a remarkably large topological Hall effect [34] attributed to skyrmions.

Inspired by these observations, we explore skyrmion crystals in a two-dimensional (2D) triangular lattice, and study the effect of a Zeeman magnetic field on the spin textures, and the impact of such spin textures on the electronic bands. Our motivation for this study is partly to understand what type of interactions can stabilize skyrmion crystals in antiferromagnets, and if broken inversion symmetry is crucial for their existence or for observing the topological Hall effect. This is expected to be an important ingredient in the search for antiferromagnetic skyrmion materials. A second motivation stems from the idea that if one can manipulate the skyrmion crystal, one can control its topological Berry flux. If this can be achieved with purely a Zeeman magnetic field, which couples to the local moments but not directly to the orbital motion of the electrons, it yields a new mechanism for quantum oscillations arising from an “emergent magnetic field”, distinct from Landau quantization in an external orbital magnetic field. We term this phenomenon “topological quantum oscillations”.

We begin with a microscopic spin model with compass and DM exchange interactions, to show that a symmetry-allowed quartic anisotropy can induce strong mode-mode coupling between the spiral spin modes and the uniform magnetization mode. In the presence of a Zeeman field, this mode coupling tunes the spiral wavevectors due to an effective renormalization of the quadratic single-ion anisotropy. This interplay leads to skyrmion lattices which are highly field-tunable; for 3D cubic multiferroic Cu_2OSeO_3 [18], this has also been experimentally reported and discussed within Landau theory [42].

In systems with dominant FM couplings and DM interactions, we find a field-induced Néel skyrmion crystal. Increasing the Zeeman field in this skyrmion crystal leads to a decrease in the magnitude of the spiral wavevector, resulting in an expansion of the skyrmion lattice. For the case with inversion symmetry (no DM interactions) and frustrating AFM couplings, we find that the Zeeman field leads to an increase in the spiral wavevector magnitude, together with an intermediate Bloch skyrmion-crystal phase, as recently observed in Gd_2PdSi_3 [34].

In the FM case, a computation of the band structures of electrons Kondo coupled to this “breathable” spin texture reveals the formation of Chern bands. Indeed, we show that this setup provides a realization of a tunable Berry-Hofstadter model driven by tunable real space Berry fluxes. Due to the field-tuning of the skyrmion lattice, we show that even a purely Zeeman magnetic field acting on the local moments leads to topological quan-

*Electronic address: arunp@physics.utoronto.ca

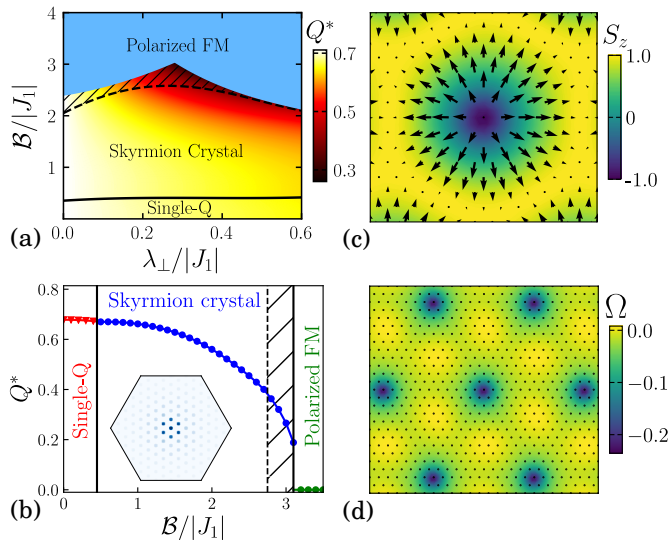


FIG. 1: (a) Phase diagram of the triangular ferromagnet with DM interaction as a function of λ_{\perp} and \mathcal{B} showing topologically trivial single- \mathbf{Q} spiral and FM phases, and nontrivial triple- \mathbf{Q} skyrmion-crystal phase. We have fixed $D = |J_1|$, $A_c = 0.4|J_1|$ and $A_s = 0.5|J_1|$. Color scale shows optimal momentum \mathbf{Q}^* in different regimes. Hatched region indicates a triple- \mathbf{Q} regime where the core spins have flipped from negative to positive magnetization before entering the polarized FM phase. This phase has a trivial total Berry flux, but is unstable after we keep a large number of harmonics and impose the hard constraint $\mathbf{S}_i^2 = 1$. (b) Field dependence of \mathbf{Q}^* , at a fixed $\lambda_{\perp} = 0.3$, displaying strong variation in the skyrmion-crystal phase. The inset shows the intensity plot of the spin structure factor inside the first Brillouin zone for a typical skyrmion crystal, featuring peaks at the center $\mathbf{Q} = 0$, the primary triple- \mathbf{Q} wavevectors and higher harmonics. (c) Structure of the Néel skyrmion with negative magnetization at the core. (d) Spatial variation of solid angle Ω subtended by three noncoplanar spins on elementary triangular plaquettes. $\Omega/4\pi$ sums to a topological charge (-1) per skyrmion.

tum oscillations in the electronic density of states. This remarkable effect, which effectively arises from scanning through this novel realization of the Hofstadter butterfly spectrum, should manifest itself in various physical observables, e.g., the electronic specific heat and transport of such skyrmion metals.

I. RESULTS

A. Model

We begin with a Hamiltonian describing classical spins on a triangular lattice, which has the key ingredients previously shown to stabilize 2D skyrmion crystals within a Landau theory [14, 24, 25]:

$$H_0 = \frac{1}{2} \sum_{i,j} J_{ij} \mathbf{S}_i \cdot \mathbf{S}_j + D \sum_{\langle ij \rangle} (\hat{z} \times \hat{r}_{ij}) \cdot (\mathbf{S}_i \times \mathbf{S}_j)$$

$$- A_c \sum_{\langle ij \rangle} (\mathbf{S}_i \cdot (\hat{z} \times \hat{r}_{ij})) (\mathbf{S}_j \cdot (\hat{z} \times \hat{r}_{ij})) - \mathcal{B} \sum_i S_{iz}. \quad (1)$$

Here J_{ij} is the Heisenberg exchange; we may choose $J_{ij} < 0$ as appropriate for a ferromagnet, or $J_{ij} > 0$ to represent a frustrated antiferromagnet. SOC induces two important anisotropic exchange interactions: A_c is a compass term which is symmetry-allowed even in the presence of inversion symmetry, while D is the chiral Rashba DM interaction which arises only when $\hat{z} \rightarrow -\hat{z}$ inversion symmetry is broken. The microscopic derivation of this term in Rashba metals has been recently revisited [43, 44]. Dresselhaus DM interaction however is not allowed by vertical-plane reflections σ_v of the triangular lattice. The Zeeman field \mathcal{B} allows for control of the ground state of the system. Increasing \mathcal{B} leads to a transition from single-mode spiral order to a triple- \mathbf{Q} skyrmion crystal, and eventually to a polarized ferromagnet at large \mathcal{B} [24, 45]. We supplement H_0 with two terms

$$H_1 = A_s \sum_i S_{iz}^2 + \lambda_{\perp} \sum_i S_{iz}^4 \quad (2)$$

Here A_s is a single-ion anisotropy which has been previously shown to influence the stability of skyrmion-crystal order [8, 14, 24, 45, 46]. The ingredient we focus on here is the local anisotropy $\lambda_{\perp} > 0$ which is the single nontrivial *quartic* coupling allowed by the C_{6v} symmetry of the lattice. As discussed below, this term leads to strong mode-mode coupling and field-tunable skyrmion lattices. Our results below are obtained via an extensive variational optimization for the skyrmion crystal solutions (see Methods).

B. Ferromagnet with DM interactions

We begin with the case of a ferromagnet with broken inversion symmetry, setting $J_{ij} = J_1 < 0$ for nearest-neighbor FM exchange, and $A_c, D \neq 0$. The resulting phase diagram, upon tuning \mathcal{B} and λ_{\perp} , is depicted in Fig. 1(a). For $\lambda_{\perp} = 0$, this is consistent with previous studies, exhibiting spiral, skyrmion crystal, and FM phases with increasing \mathcal{B} [24]. Our key observation is that incorporating $\lambda_{\perp} \neq 0$ leads to a qualitatively similar phases. The key difference is that the primary wavevectors \mathbf{Q}^* , which lie in the Γ - M directions, now exhibit a strong field dependence, as seen from Fig. 1(b). This leads to a strong field dependence of the skyrmion-crystal lattice constant. We trace this dependence of \mathbf{Q}^* on \mathcal{B} to an effective renormalization of the easy-plane anisotropy. This is heuristically seen from a Hartree-level treatment [42] of the λ_{\perp} quartic term, which yields $A_s^{\text{eff}} = A_s + 6\lambda_{\perp} m_0^2$, where m_0 increases with increasing \mathcal{B} . This renormalization of A_s leads to a change in the optimal \mathbf{Q}^* , thus tuning the skyrmion crystal (see Supplemental Material).

The spin texture stabilized in this system is a lattice of Néel skyrmions as depicted in Fig. 1(c). We find that

the solid angle Ω subtended by the three spins on each elementary triangular plaquette shows a strong spatial variation, being higher at the skyrmion core, as seen from Fig. 1(d). (In the continuum, $\Omega = \mathbf{S} \cdot \partial_x \mathbf{S} \times \partial_y \mathbf{S}$.) Adding up $\Omega/4\pi$ across the lattice, we obtain an average topological charge (-1) per skyrmion. When the Zeeman field enhances the skyrmion-crystal lattice constant, this flux gets distributed over a larger area. We thus expect electrons moving in such a spin-textured background to sense an average “emergent orbital field” which decreases as we increase the Zeeman field on the local moments.

C. Inversion symmetric antiferromagnets

We next turn to the antiferromagnet Gd_2PdSi_3 , where recent experiments have reported nontrivial spin textures via the discovery of a large topological Hall effect at intermediate applied magnetic fields [34]. Gd_2PdSi_3 has a layered structure with triangular lattices of Gd moments spaced apart by metallic Pd/Si layers. In each Pd/Si layer, the Pd and Si atoms could form a superstructure with a quadrupled unit cell [34]. We find this leads to bond-dependent DM interactions; for simplicity, we ignore such spatially varying DM terms, and instead assume a homogeneous random configuration or a short-correlation length superstructure for the Pd and Si atoms. The crystal structure then has inversion symmetry on average about the Gd-Gd bond centers, and the DM exchange interactions between the Gd moments can then be dropped, thus simplifying our model Hamiltonian. However, we retain the compass anisotropy which is symmetry-allowed (even when inversion symmetry is present) and appears to be important for magnetism in Gd_2PdSi_3 . Magnetic resonant X-ray scattering (RXS) [34] has found evidence for incommensurate magnetic order with wavevectors along Γ - M line in the hexagonal BZ. Such magnetic ordering could arise from interactions mediated by the conduction electrons.

To understand these observations, we study the Hamiltonian $H_0 + H_1$ from Eqns.1,2, applied to a single triangular Gd layer embedded in the crystal, with FM nearest-neighbor exchange $J_1 < 0$ and large AFM frustrating next-neighbor exchange $J_2 > 0$. Inversion symmetry leads to the absence of a DM interaction between Gd moments, thus $D = 0$. However, a compass term is permitted, so we set $A_c \neq 0$. Our work goes beyond previous studies of skyrmions in this frustrated magnetic Hamiltonian [30, 31] by incorporating the impact of symmetry-allowed quartic couplings as well as compass terms. As in the FM example, we have examined variational single- \mathbf{Q} and multi- \mathbf{Q} orders for the ground state of this AFM Hamiltonian (see Methods). We thus arrive at the phase diagram shown in Fig. 2(a). We find in this case that the zero-field single- \mathbf{Q} spiral order gives way to a triple- \mathbf{Q} state with increasing \mathcal{B} , which in turn gives way to a double- \mathbf{Q} state. This sequence of phases is qualitatively consistent with the magnetic RXS results [34]. The even-

tual polarized ferromagnet appears at much higher fields $\mathcal{B} \gtrsim 30|J_1|$, which has not been accessed in experiments at the lowest temperature. Interestingly, we find that the characteristic wavevector Q^* of the spirals making up the spin texture increases slightly in this case as we increase \mathcal{B} as shown in Fig. 2(b). Precisely such a trend has been observed in Gd_2PdSi_3 [34]. With increasing field, the intensity in the FM component increases, while the intensity in the incommensurate wavevectors decreases.

The real-space spin texture in the intermediate-field triple- \mathbf{Q} state is shown in Fig. 2(c). We find that the crystal is made of Bloch skyrmions in a ferromagnetic background. Fig. 2(d) shows the spatial variation of the solid angle Ω subtended by the three noncoplanar spins on each elementary triangular plaquette, with the circles indicating the cores of the skyrmions. Summing $\Omega/4\pi$ over the magnetic unit cell yields a net topological charge (-1) per skyrmion. In this AFM case, due to the shorter length scale associated with the spin texture, the distinction between the interskyrmion separation and the magnetic unit cell periodicity alluded to earlier is clearly visible in the spatial structure of the texture as well as Ω . For instance, Ω around each skyrmion core has a slightly different pattern, and the periodicity is only recovered at a longer length scale of the magnetic unit cell.

Here, the skyrmion crystal is stabilized by the interplay between the quadratic and the quartic anisotropy terms, A_s and λ_\perp respectively, while a nonzero A_c is needed to get a tunable Q^* . We find $A_c > 0$ favors Néel-type skyrmion crystals, while $A_c < 0$ stabilizes Bloch-type skyrmion crystals; however, only the latter also leads to the observed enhancement of Q^* with field. We thus expect $A_c < 0$, and predict that the experiments should observe a lattice of Bloch skyrmions. More importantly, if we assume $A_c = 0$, the Hamiltonian for this classical spin system has a global symmetry under which we can flip all $S_x \rightarrow -S_x$ or $S_y \rightarrow -S_y$. This operation also flips the skyrmion topological charge [30]. Since the real crystal would then be expected to have equal number of domains of this spontaneously broken symmetry, this would lead to a zero average topological Hall effect. This is in striking contrast to the observed large topological Hall effect. We thus identify a nonzero compass exchange term, which explicitly breaks this global spin flip symmetry and selects a specific charge $Q = -1$ for the skyrmion, as a crucial ingredient for observing a nonzero topological Hall effect in centrosymmetric frustrated magnets.

D. Topological quantum oscillations

We finally turn to the nature of electronic bands which emerge from coupling conduction electrons to highly tunable skyrmion lattices, focussing here on ferromagnets with DM exchange. We consider a nearest-neighbor ordinary hopping t and Rashba hopping χ_R for the conduction electrons, and assume that the electrons sense the underlying spin texture $\{\mathbf{S}_i\}$ via a ferromagnetic Kondo

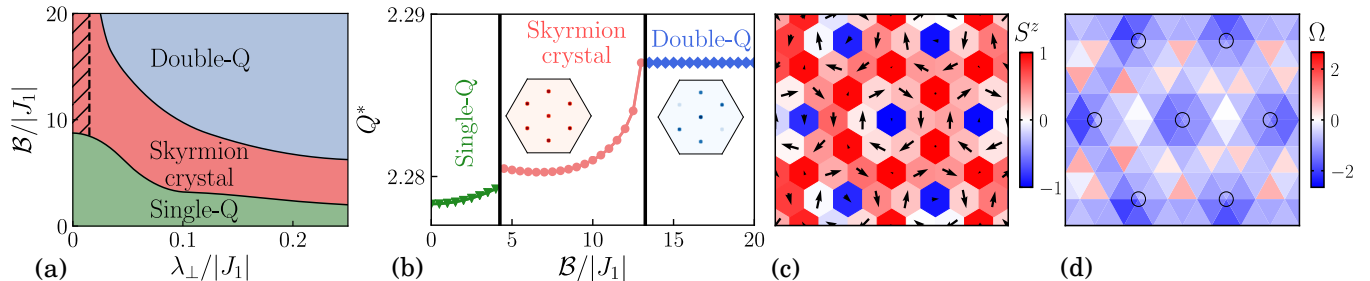


FIG. 2: (a) Phase diagram of the triangular AFM model with compass term as a function of quartic anisotropy λ_{\perp} and field B for fixed $A_s = -0.25|J_1|$, $A_c = -0.2|J_1|$ and $J_2 = 4|J_1|$. With increasing B at fixed λ_{\perp} , we find an evolution from single- \mathbf{Q} to a skyrmion crystal to a double- \mathbf{Q} phase. The hatched region is a trivial triple- \mathbf{Q} phase, featuring a triangular array of negative-magnetization islands in a positive-magnetization background, similar to the “bubble crystal” studied in Ref.[47]. (b) Evolution of the wavevector \mathbf{Q}^* with B . Both (a) and (b) are qualitatively consistent with data on Gd_2PdSi_3 . The insets are typical intensity plots of the spin structure factors inside the first Brillouin zone for the skyrmion crystal phase and the double- \mathbf{Q} phase. (c) Spin texture in the skyrmion-crystal phase, showing Bloch skyrmions (centered on blue hexagons) in a ferromagnetic background. (d) Spatial variation of the solid angle Ω subtended by the three spins on elementary triangular plaquettes; circles denote the skyrmion cores. Summing $\Omega/4\pi$ yields an average topological charge (-1) per skyrmion.

interaction $J_H > 0$ [32, 37] which can physically arise from atomic Hund’s coupling (see Methods for details). The resulting number of electronic bands depends on the skyrmion lattice. If we pick $\mathbf{Q}^* = (4\pi/\sqrt{3})(m/n)\hat{y}$ (and its symmetry-allowed partners) as the best approximant to the optimal spin-crystal wavevector, the periodic “magnetic unit cell” of the triple- \mathbf{Q} state has n^2 triangular lattice sites and encloses m^2 skyrmions. This hosts $2n^2$ bands including spin.

This commensurability effect of the skyrmion lattice with the underlying crystal lattice does not appear in continuum field theories. It has also not been discussed in previous work on lattice models, since these have only studied the simplest example with fixed $m = 1$ [32, 33]. Here, and more clearly in the AFM model below, we will see that this more general case results in the Berry flux, and indeed all local observables, exhibiting small modulations from one skyrmion to the next, with periodicity recovered over the magnetic unit cell. Crucially, we find that adding up the solid angles subtended by the three spins on an elementary plaquettes leads to a quantized result, in units of 4π , only when we sum over *all* m^2 skyrmions in the magnetic unit cell. Thus, the topological charge per skyrmion is quantized to (-1) only when averaged over the full magnetic unit cell.

The resulting band dispersions for $\chi_R/t = 0, \pm 0.1$ and $J_H/t = 5$ are shown along high-symmetry paths in the BZ in Fig. 3(a). The plotted bands correspond to half of all the $2n^2$ bands, where conduction-electron spins are aligned with the local moments. In all cases, these low-energy bands appear isolated and have Chern number $C = -1$, resembling somewhat dispersive Landau levels. Thus, at special electronic densities which fill up an integer number of these bands, we would expect a large quantized topological Hall effect [32, 33]. The high-energy bands come in pairs due to band sticking along the high-symmetry Γ - M line; in this case the total Chern

number of the pair is $C_{\text{pair}} = -2$. In an intermediate-energy window, around $E/t \approx -3$, we find a set of bands carrying large positive Chern numbers $C \gg 1$, which ensures that the Chern numbers over all bands sum to zero. For $|\chi_R| \ll t$, this occurs around the van-Hove singularity in the density of states (DOS) of the triangular lattice, where a Lifshitz transition occurs near the M -point. This distribution of Chern numbers is analogous to that for the Hofstadter model [33].

Fig. 3(b) plots the electronic DOS at the Fermi level as we vary the Zeeman field B on the local moments, staying at a fixed electron density $\rho = 0.1$ electrons per site of the original triangular lattice. Despite the low energy Chern bands having some dispersion, we find that the DOS shows clear topological quantum oscillations, even though the electrons are not subject to any direct orbital magnetic field! The oscillations can be understood by observing that the expansion of the skyrmion lattice leads to a decrease in the average Berry flux density. This problem is thus analogous to studying a Hofstadter model with a decreasing magnetic flux ϕ per plaquette [48, 49]. In the conventional Hofstadter problem, varying ϕ leads to a rich Hofstadter butterfly spectrum due to the interplay of two length scales — set by the unit cell area of the underlying lattice and the area of the magnetic unit cell. In our problem, the role of ϕ is effectively played by $Q^{*2} = [(4\pi/\sqrt{3})(m/n)]^2$. As the Zeeman field B is tuned, Q^* changes, and the oscillations in the DOS can thus be identified with a scan in ϕ through the Hofstadter butterfly spectrum. Our model differs from the conventional Hofstadter model in that the flux per plaquette is not really uniform, and there exists a third length scale — the skyrmion size — characterizing the spatial inhomogeneity of the emergent “orbital magnetic field”.

These topological DOS oscillations should impact all physical observables. Since we are tuning the Zeeman field B on the local moments, this nontrivial effect is

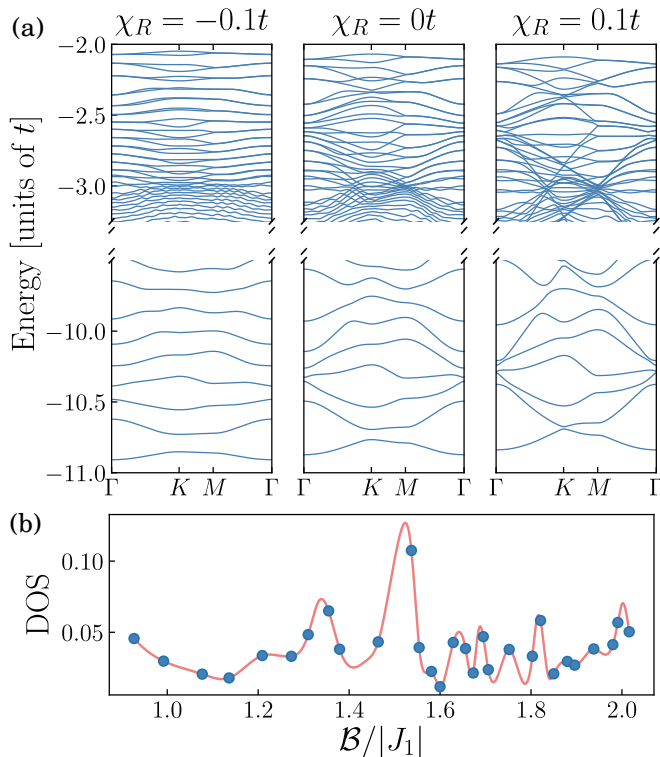


FIG. 3: (a) Band structure along high-symmetry paths in the hexagonal BZ in the skyrmion-crystal phase for the ferromagnet with DM interactions. The conduction electrons are assumed to have ordinary hopping t , a Rashba hopping $\chi_R = 0, \pm 0.1t$, with a coupling to the localized spins via ferromagnetic exchange $J_H/t = 5$. The plotted bands correspond to half of all the bands, where conduction-electron spins are aligned with the local moments. The low-energy bands are well isolated, and carry Chern numbers -1 . The high-energy bands come in pairs, exhibiting band sticking along Γ - M , with total Chern number $C_{\text{pair}} = -2$. Finally, there are a set of bands near $E \approx -3t$ which are connected and carry large $C > 0$ Chern numbers to ensure that the total Chern number is zero. (b) Oscillations in the DOS at the Fermi level (in units of t^{-1}) for $\chi_R = 0$ and fixed conduction electron density $\rho = 0.1$ electrons per site. These topological quantum oscillations arise from the \mathcal{B} dependence of Q^* .

distinct from previous studies which simply varied the electron filling in a fixed skyrmion texture. The oscillations we describe would be further impacted by the direct Zeeman and orbital effects of the magnetic field on the conduction electrons; however, the typically much stronger effect of the skyrmion lattice and its Berry flux should still lead to observable effects as deviations from conventional quantum oscillations in skyrmion magnets.

II. DISCUSSION

We have studied magnetic skyrmions in 2D FM and AFM systems, arguing that quartic anisotropies can lead

to field tunable skyrmion crystals. Such anisotropies can arise from single-ion physics or from integrating out conduction electrons. For the FM case, where this field tunability is highly pronounced, we have shown that topological quantum oscillations can arise from just the impact of a Zeeman field on the local moments. The Chern bands which contribute to these oscillations are already somewhat dispersive; we thus expect disorder broadening which is weaker than the scale of this bandwidth (which is also comparable to the band gap) will not alter our main results. The amplitude of these topological oscillations are not expected to follow simple Lifshitz-Kosevich scaling since, unlike Landau levels, the emergent Chern bands are not flat and equispaced in energy. The physics underlying these topological quantum oscillations is not crucially dependent on the triangular lattice symmetry - thus, a heterostructure with an ultrathin metallic film deposited on insulating Cu_2OSeO_3 , where a field-tunable skyrmion crystal has been reported [42], may be a potential venue for observing this effect. Further experimental and theoretical work on such a proposed heterostructure would thus be valuable, in assessing the viability of our proposal, as would searches for more promising material candidates. For the AFM case, we have found that we can qualitatively understand recent observations of multi- \mathbf{Q} orders reported in Gd_2PdSi_3 crystals. We have shown that the field dependence of the skyrmion wavevector and the subtlety in understanding the experimentally measured large topological Hall effect in the intermediate skyrmion crystal phase can be consistently resolved from the interplay of magnetic frustration and various anisotropies including compass exchange terms.

III. METHODS

A. Variational optimization for skyrmion crystal

To study the ground states of the Hamiltonian $H_0 + H_1$, we resort to a variational approach. We begin by imposing the spin-length constraint $\mathbf{S}_i^2 = 1$ on average, setting $\sum_i \mathbf{S}_i^2 = N$ where N is the number of sites. For $\lambda_\perp = \mathcal{B} = 0$, a Luttinger-Tisza analysis yields degenerate spin-spiral solutions. We therefore consider a general ansatz $\mathbf{S}_i = \mathbf{m}_0 + \sum_n \mathbf{m}_n e^{i\mathbf{Q}_n \cdot \mathbf{r}_i}$, retaining the uniform component \mathbf{m}_0 , and a set of symmetry-equivalent spirals with wavevectors \mathbf{Q}_n and amplitudes \mathbf{m}_n .

The simplest skyrmion lattice is constructed from a set of three primary spiral wavevectors which sum to zero (in addition to the FM mode), i.e. it is a triple- \mathbf{Q} spin crystal. The impact of the hard-spin constraint and the nonlinear coupling $\lambda_\perp \neq 0$ is to generate higher harmonics of these primary \mathbf{Q} 's [10]. The full variational state is obtained by optimizing the ansatz for $\{\mathbf{m}_0, \mathbf{m}_n, \mathbf{Q}_n\}$ (cutoff at a certain order in the harmonics), followed by explicitly normalizing the spin vector at each site. See Supplemental Material for details.

B. Band structure of conduction electrons

To study the influence of the skyrmion crystal on conduction electrons, we have diagonalized a Hamiltonian for electrons on the triangular lattice (same lattice as the spins),

$$H_{\text{elec}} = -\sum_{j,\ell} t_{j\ell} c_{j\alpha}^\dagger c_{\ell\alpha} - \sum_{j,\ell} i\chi_R^{(j\ell)} c_{j\alpha}^\dagger [\hat{z} \times \hat{r}_{j\ell} \cdot \vec{\sigma}]_{\alpha\beta} c_{\ell\beta} - J_H \sum_j \mathbf{S}_j \cdot c_{j\alpha}^\dagger \vec{\sigma}_{\alpha\beta} c_{j\beta}. \quad (3)$$

We have considered magnetic unit cells of up to $n^2 = 3600$ sites with varying \mathcal{B} , and diagonalized the corresponding $2n^2 \times 2n^2$ electronic Hamiltonian at all momenta \mathbf{k} in the reduced hexagonal Brillouin zone (BZ) of the skyrmion crystal. To compute the Chern number of the electronic bands, we have considered a fine mo-

mentum discretization in the BZ, and used the method discussed in Ref.50.

Acknowledgments: We acknowledge insightful discussions with Achim Rosch. Computations were performed on the Niagara supercomputer at the SciNet HPC Consortium. SciNet is funded by: the Canada Foundation for Innovation under the auspices of Compute Canada; the Government of Ontario; Ontario Research Fund - Research Excellence; and the University of Toronto.

Contributions: AP proposed the project. SS and SD devised and carried out the calculations in discussion with AP. All three authors participated in preparation of the manuscript.

Competing interests: The authors declare that they have no competing interests.

Funding: This research was funded by NSERC of Canada and the Canadian Institute for Advanced Research.

-
- [1] T. Skyrme, Nuclear Physics **31**, 556 (1962).
[2] S. L. Sondhi, A. Karlhede, S. A. Kivelson, and E. H. Rezayi, Phys. Rev. B **47**, 16419 (1993).
[3] H. A. Fertig, L. Brey, R. Côté, and A. H. MacDonald, Phys. Rev. B **50**, 11018 (1994).
[4] S. E. Barrett, G. Dabbagh, L. N. Pfeiffer, K. W. West, and R. Tycko, Phys. Rev. Lett. **74**, 5112 (1995).
[5] Y. P. Shkolnikov, S. Misra, N. C. Bishop, E. P. De Poortere, and M. Shayegan, Phys. Rev. Lett. **95**, 066809 (2005).
[6] A. Bogdanov and A. Hubert, Sov. Phys. JETP **68**, 101 (1989).
[7] A. Bogdanov and A. Hubert, Journal of Magnetism and Magnetic Materials **138**, 255 (1994).
[8] A. N. Bogdanov, U. K. Röbller, M. Wolf, and K.-H. Müller, Phys. Rev. B **66**, 214410 (2002).
[9] U. K. Röbller, A. N. Bogdanov, and C. Pfleiderer, Nature **442**, 797 EP (2006).
[10] B. Binz, A. Vishwanath, and V. Aji, Phys. Rev. Lett. **96**, 207202 (2006).
[11] B. Binz and A. Vishwanath, Phys. Rev. B **74**, 214408 (2006).
[12] S. Mühlbauer, B. Binz, F. Jonietz, C. Pfleiderer, A. Rosch, A. Neubauer, R. Georgii, and P. Böni, Science **323**, 915 (2009).
[13] X. Z. Yu, Y. Onose, N. Kanazawa, J. H. Park, J. H. Han, Y. Matsui, N. Nagaosa, and Y. Tokura, Nature **465**, 901 EP (2010).
[14] A. B. Butenko, A. A. Leonov, U. K. Röbller, and A. N. Bogdanov, Phys. Rev. B **82**, 052403 (2010).
[15] S. Heinze, K. von Bergmann, M. Menzel, J. Brede, A. Kubetzka, R. Wiesendanger, G. Bihlmayer, and S. Blügel, Nature Physics **7**, 713 EP (2011).
[16] T. Schulz, R. Ritz, A. Bauer, M. Halder, M. Wagner, C. Franz, C. Pfleiderer, K. Everschor, M. Garst, and A. Rosch, Nature Physics **8**, 301 EP (2012).
[17] A. Tonomura, X. Yu, K. Yanagisawa, T. Matsuda, Y. Onose, N. Kanazawa, H. S. Park, and Y. Tokura, Nano Letters **12**, 1673 (2012).
[18] S. Seki, X. Z. Yu, S. Ishiwata, and Y. Tokura, Science **336**, 198 (2012).
[19] S. Hayami and Y. Motome, Phys. Rev. Lett. **121**, 137202 (2018).
[20] K. N. Okada, Y. Kato, and Y. Motome, ArXiv e-prints (2018), 1809.07582.
[21] W. Jiang, P. Upadhyaya, W. Zhang, G. Yu, M. B. Jungfleisch, F. Y. Fradin, J. E. Pearson, Y. Tserkovnyak, K. L. Wang, O. Heinonen, et al., Science **349**, 283 (2015).
[22] A. S. Ahmed, B. D. Esser, J. Rowland, D. W. McComb, and R. K. Kawakami, Journal of Crystal Growth **467**, 38 (2017).
[23] A. S. Ahmed, J. Rowland, B. D. Esser, S. R. Dunsiger, D. W. McComb, M. Randeria, and R. K. Kawakami, Phys. Rev. Materials **2**, 041401 (2018).
[24] S. Banerjee, J. Rowland, O. Erten, and M. Randeria, Phys. Rev. X **4**, 031045 (2014).
[25] X. Li, W. V. Liu, and L. Balents, Phys. Rev. Lett. **112**, 067202 (2014).
[26] J. Matsuno, N. Ogawa, K. Yasuda, F. Kagawa, W. Koshibae, N. Nagaosa, Y. Tokura, and M. Kawasaki, Science Advances **2** (2016).
[27] A. Neubauer, C. Pfleiderer, B. Binz, A. Rosch, R. Ritz, P. G. Niklowitz, and P. Böni, Phys. Rev. Lett. **102**, 186602 (2009).
[28] N. Kanazawa, Y. Onose, T. Arima, D. Okuyama, K. Ohoyama, S. Wakimoto, K. Kakurai, S. Ishiwata, and Y. Tokura, Phys. Rev. Lett. **106**, 156603 (2011).
[29] I. Martin and C. D. Batista, Phys. Rev. Lett. **101**, 156402 (2008).
[30] T. Okubo, S. Chung, and H. Kawamura, Phys. Rev. Lett. **108**, 017206 (2012).
[31] A. O. Leonov and M. Mostovoy, Nature Communications **6**, 8275 EP (2015).
[32] K. Hamamoto, M. Ezawa, and N. Nagaosa, Phys. Rev. B **92**, 115417 (2015), 1504.06024.
[33] B. Göbel, A. Mook, J. Henk, and I. Mertig, Phys. Rev. B **95**, 094413 (2017).
[34] T. Kurumaji, T. Nakajima, M. Hirschberger,

- A. Kikkawa, Y. Yamasaki, H. Sagayama, H. Nakao, Y. Taguchi, T.-h. Arima, and Y. Tokura, ArXiv e-prints (2018), 1805.10719.
- [35] G. E. Volovik, *Journal of Physics C: Solid State Physics* **20**, L83 (1987).
- [36] J. Ye, Y. B. Kim, A. J. Millis, B. I. Shraiman, P. Majumdar, and Z. Tešanović, *Phys. Rev. Lett.* **83**, 3737 (1999).
- [37] K. Ohgushi, S. Murakami, and N. Nagaosa, *Phys. Rev. B* **62**, R6065 (2000).
- [38] H. D. Rosales, D. C. Cabra, and P. Pujol, *Phys. Rev. B* **92**, 214439 (2015).
- [39] Y. Kato, I. Martin, and C. D. Batista, *Phys. Rev. Lett.* **105**, 266405 (2010).
- [40] B. Göbel, A. Mook, J. Henk, and I. Mertig, *New Journal of Physics* **19**, 063042 (2017).
- [41] Mallik, R., Sampathkumaran, E. V., Strecker, M., and Wortmann, G., *Europhys. Lett.* **41**, 315 (1998).
- [42] A. Chacon, L. Heinen, M. Halder, A. Bauer, W. Simeth, S. Mühlbauer, H. Berger, M. Garst, A. Rosch, and C. Pfleiderer, *Nature Physics* **14**, 936 (2018).
- [43] I. A. Ado, A. Qaiumzadeh, R. A. Duine, A. Brataas, and M. Titov, *Phys. Rev. Lett.* **121**, 086802 (2018).
- [44] A. Qaiumzadeh, I. A. Ado, R. A. Duine, M. Titov, and A. Brataas, *Phys. Rev. Lett.* **120**, 197202 (2018).
- [45] J. Rowland, S. Banerjee, and M. Randeria, *Phys. Rev. B* **93**, 020404 (2016).
- [46] A. O. Leonov, ArXiv e-prints (2014), 1406.2177.
- [47] S. Hayami, S.-Z. Lin, and C. D. Batista, *Phys. Rev. B* **93**, 184413 (2016).
- [48] D. Weiss, K. von Klitzing, K. Ploog, and G. Weimann, *Surface Science* **229**, 88 (1990).
- [49] L. A. Chizhova, F. Libisch, and J. Burgdörfer, *Phys. Rev. B* **90**, 165404 (2014).
- [50] T. Fukui, Y. Hatsugai, and H. Suzuki, *Journal of the Physical Society of Japan* **74**, 1674 (2005).